Available online at www.sciencedirect.com

ScienceDirect

journal homepage: www.elsevier.com/locate/he

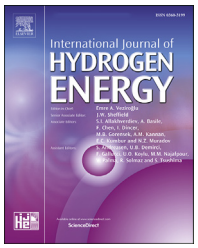

Optimal Ni loading towards efficient CH_4 production from H_2 and CO_2 over Ni supported onto fibrous SBA-15

S.N. Bukhari [a], C.C. Chong [a], H.D. Setiabudi [a,b,*], N. Ainirazali [a], M.A.A. Aziz [c,d], A.A. Jalil [d,e], S.Y. Chin [a,b]

[a] Faculty of Chemical and Natural Resources Engineering, Universiti Malaysia Pahang, 26300 Gambang, Kuantan, Pahang, Malaysia

[b] Centre of Excellence for Advanced Research in Fluid Flow, Universiti Malaysia Pahang, 26300 Gambang, Kuantan, Pahang, Malaysia

[c] Sustainable Waste Management Research Group, Faculty of Chemical and Energy Engineering, Universiti Teknologi Malaysia, UTM, 81310 Johor Bahru, Johor, Malaysia

[d] School of Chemical and Energy Engineering, Faculty of Engineering, Universiti Teknologi Malaysia, 81310 UTM, Johor Bahru, Johor, Malaysia

[e] Centre of Hydrogen Energy, Institute of Future Energy, Universiti Teknologi Malaysia, UTM, 81310 Johor Bahru, Johor, Malaysia

ARTICLE INFO

Article history:
Received 6 October 2018
Received in revised form
24 January 2019
Accepted 27 January 2019
Available online 23 February 2019

Keywords:
Ni/F-SBA-15
Methane
Ni loadings
Metal-support interaction
Coke deposition

ABSTRACT

The transformation of SBA-15 into fibrous type SBA-15 (F-SBA-15) as well as the influence of Ni loadings (1, 3, 5, and 10 wt%) towards an efficient CH_4 production from H_2 and CO_2 were explored. The synthesized catalysts were characterized using XRD, BET, ICP-MS, FTIR, FESEM-EDX, TEM, and in-situ FTIR adsorbed pyrrole. Increasing Ni loadings onto F-SBA-15 support promoted excellent performance towards CO_2 methanation. The efficacy in CO_2 methanation over Ni/F-SBA-15 increased with a sequence of 1%Ni/F-SBA-15 < 3%Ni/F-SBA-15 < 5%Ni/F-SBA-15 ≈ 10%Ni/F-SBA-15, indicating the superior performance and stability of 5%Ni/F-SBA-15. The increasing trend was due to the fibrous morphology of support which enhanced the quantity of Si–O–Ni bond, triggered better Ni dispersion, strengthen metal-support interaction, and increased the basicity. However, higher Ni loadings (10 wt %) onto F-SBA-15 slightly declined the performance and stability of CO_2 methanation due to the limited spaces for substitution of Ni species with the silanol groups of F-SBA-15 upon the bulk Ni phase, poorer Ni dispersion, weaker metal-support interaction, and lower basicity. The new finding of combination between fibrous SBA-15 (F-SBA-15) with an optimum Ni loading contributed towards an outstanding performance and thus could be applied in various applications.

* *Corresponding author*. Faculty of Chemical and Natural Resources Engineering, Universiti Malaysia Pahang, 26300 Gambang, Kuantan, Pahang, Malaysia.
E-mail address: herma@ump.edu.my (H.D. Setiabudi).

https://doi.org/10.1016/j.ijhydene.2019.01.259

Introduction

Energy crisis that related to an excess consumption of fossil fuels (e.g. coal, oil, natural gas) as well as its very limited reserves of the fuels nowadays is one of the main concerns in this recent year owing to it can eventually cause the great risk for the future whereby it may run out in the coming decades. Many approaches have been drawn towards the mitigation of this energy crisis into the shortage of fossil fuels, and even as the renewable energy storage that generates the electricity production in power plant including the H_2 generation from biomass gasification [1], hydrolysis of $NaZn(BH_4)_3$ and its ammoniates [2], and ethanol steam reforming of MMT-supported Ni/TiO_2 nanocomposite [3] as well as the CH_4 production from the hydrogenation of CO_2 using supported metal catalysts [4,5]. Among the different pathway of energy and fuels formation, CO_2 methanation (as shown in Eq. (1)) is considered as one of the most feasible and plausible reaction routes owing to its CO_2 utilisation into more valuable, marketable and economical products such as methane (CH_4). Additionally, considering the infrastructure for transport and storage of CH_4 is already present, the CH_4 produced by this reaction can be easily sent to the chemical industries and can even be utilized as an energy vector. However, the most suitable catalyst is needed for the CO_2 methanation reaction.

$$CO_2 + 4H_2 \leftrightarrow CH_4 + 2H_2O \quad (1)$$

For the choice of support, the most widely used family of mesoporous silica material types are Santa Barbara Amorphous No. 15 (SBA-15) and Mobil Composition of Matter No. 41 (MCM-41) [6–8]. However, the mesoporous SBA-15 is extensively preferred as the most promising support for the preparation of supported metal catalysts owing to its favorable textural characteristics with greater surface area (600–1000 $m^2\ g^{-1}$), bigger pore size diameter (5–30 nm), thicker pore walls (3–6 nm), higher thermal and hydrothermal stability as well as highly uniform-arranged mesopores [8]. Nickel (Ni) is selected as the type of metal to be incorporated with the support owing to its low price, easily available, and high catalytic performance [9,10]. Even though Ni-based catalyst has been extensively used in CH_4 production, the conventional Ni-based catalyst is not promising as it suffers from severe limitations. This type of catalyst is always accompanied by carbon deposition and metal sintering even at the low reaction temperature. In addition, the agglomeration of metal is sometimes difficult to control and thus results in a weak metal-support interaction and low catalytic activity and stability [11].

Recently, a few researchers discovered the superior catalytic performance and stability over metal supported onto fibrous morphology of ordered mesoporous silica material [9.10]. The development of support with fibrous morphology and dendrimeric structure has become attractive due to a homogenous and better metal dispersion onto support, producing a promising well-dispersed metal-based fibrous catalyst. Previously, Fihri et al. [12] found that the fibrous type of nano-silica (KCC-1) improved the distribution of Ru particles and thus resulted in a superior performance towards alkane hydrogenolysis and hindered the deactivation activity of the catalyst even after eight days. This promising catalytic performance was related to the restriction of Ostwald ripening of Ru nanoparticles when they were dispersed into the fibrous type of KCC-1. In addition, the fibrous type of support with the dendrimeric structure also gains several attentions due to its advantages in allowing a bulky mass of reactants to interact with the active sites of the catalyst [13]. Notably, this favorable fibrous structure of mesoporous silica materials is expected to be as a promising candidate to produce a homogenous and well-dispersed Ni-based catalyst. To the best of our knowledge, no study has been done on the fabrication structure of SBA-15 into fibrous morphology (F-SBA-15). Herein, this study highlighted on the modification structure of SBA-15 support into novel fibrous type (F-SBA-15) in order to produce a higher accessibility of metal to be dispersed onto the pores of support due to its formation of a dendrimeric structure.

Instead of the morphology of support, the amount of metal loadings on the support also influences the behavior and stability of the catalyst. Previously, few researchers reported the vital role of an optimum amount of metal loading in the enhancement of numerous reactions including CO_2 methanation [14], ethanol steam reforming [3], and CO_2 reforming of CH_4 [15] due to the higher accessibility and better metal dispersion as well as stronger metal-support interaction. They also reported that the optimum amount of metal loading will influence the less occurrence of migration and metal sintering on the channels of support during the reaction. Thus, the amount of metal loading is considered as the significant effect that need to be examined for preparing the good behavior and stability of Ni/F-SBA-15 towards CO_2 methanation.

The combination of a modified fibrous type of SBA-15 (F-SBA-15) with the different amount of Ni loadings (1, 3, 5, and 10 wt%) was explored as to determine the influences and limitations of emerging the physical properties of metal-based fibrous catalyst towards a superior catalytic performance. In addition, the stability of the catalyst towards efficient CH_4 production with the minimum occurrence of metal sintering was also studied. The properties of all synthesized Ni/F-SBA-15 were determined using XRD, BET, ICP-MS, FTIR, FESEM-EDX, TEM, and in-situ FTIR adsorbed pyrrole, meanwhile all spent Ni/F-SBA-15 were evaluated by XRD and TGA analysis.

Materials and methods

Catalysts preparation

According to Zhao et al. [8], SBA-15 synthesis was done by mixing and stirring the triblock copolymer poly (ethylene glycol)-poly (propylene glycol)-poly (ethylene glycol) (PEO-PPO-PEO/P123) (Sigma-Aldrich, average molecular weight = 5800) with an aqueous solution of 2 M hydrochloric acid (HCl, 37 wt%) at 313 K for 1 h, followed by adding with the tetraethylorthosilicate (Merck, TEOS) (mass ratio of TEOS/P123 = 2.21). The resulting solution was stirred for another 24 h at 313 K, and subsequently treated under hydrothermal condition using reflux hydrothermal treatment method for 4 h at 353 K. The obtained white precipitate was filtered, rinsed

thoroughly with deionized water, oven-dried (383 K, 12 h), and calcined (823 K, 3 h).

The surface modification of SBA-15 was executed by microemulsion solution method coupled with SBA-15 crystal-seed crystallization method as referred to the previous methodology reported by Firmansyah et al. [13]. A homogenous solution of tetraethylorthosilicate (Merck, TEOS), *n*-butanol (Merck) and toluene (Sigma-Aldrich) were mixed, followed by adding with SBA-15 powder (calcined) under stirring for 30 min at ambient temperature. The mixture of hexadecyltrimethylammonium bromide (CTAB, Sigma-Aldrich, $\geq$ 98%), urea (Merck, $CO(NH_2)_2$), and deionized water was stirred and then dropped on the first prepared solution under stirring at ambient temperature for another 3 h. The resulting solution was put into a Teflon-lined stainless-steel autoclave for hydrothermal heating at 353 K for 4 h. The solid product of F-SBA-15 was centrifuged, washed thoroughly with deionized water, oven-dried (383 K, 12 h), and calcined (823 K, 6 h).

Ni/F-SBA-15 was then synthesized by incipient wetness impregnation method. The synthesized F-SBA-15 was dispersed with the aqueous solution of $Ni(NO_3)_2 \cdot 6H_2O$ (Merck, 99%), and subsequently stirred at 353 K until almost all the water was being evaporated. Then the product was dried (383 K, 12 h) and calcined (823 K, 3 h). Ni loadings used in this study were 1, 3, 5, and 10 wt%.

Catalysts characterization

X-ray diffraction (XRD) analysis was carried out for the identification of crystalline structure using Philips X' Pert MPD, 3 kW that equipped with Cu Kα radiation ($\lambda = 1.5405$ Å). The evaluation of NiO crystallite size (D_{NiO}) was done based on the Scherrer equation [16]. XRD analysis was also used for the evaluation of the spent catalysts properties.

$$D_{NiO} = \frac{0.9\lambda}{B \cos \theta} \quad (2)$$

Analysis of the textural characteristics (i.e., BET surface area and porosity) of the catalysts was evaluated using Bruneuer-Emmett-Teller (BET) (AUTOSORB-1 model AS1 MP-LP instrument). The specimens were evacuated at 473 K for 4 h. The determination of the specific BET surface area and the porosity of catalysts were done based on the BET equation and Barrett-Joyner-Halenda (BJH) method, respectively.

The validation of exact amount of Ni loadings that were dispersed onto F-SBA-15 support was performed by using the inductively coupled plasma mass spectrometry (ICP-MS). The actual Ni loadings were compared with the intended Ni loadings.

Agilent Cary 640 Fourier Transform Infrared (FTIR) Spectrometer was used for the determination of functional groups and chemical bonding of F-SBA-15 and Ni/F-SBA-15 using the KBr matrix within the scan range of 500–1400 cm^{-1} with a resolution of 5 cm^{-1}. The pellet was prepared by mixing 1 mg of catalyst with 100 mg of KBr. Meanwhile, the basicity of the catalysts was identified using in-situ FTIR adsorbed pyrrole analysis. 30 mg of the catalyst prepared as a self-supported wafer was loaded into a high-temperature stainless steel cell with CaF_2 windows and reduced at 673 K for 1 h, followed by cooling to ambient temperature. Then, the activated catalyst was introduced to 4 Torr of pyrrole at ambient temperature for 5 min, and subsequently evacuated at ambient temperature, 323 K, 373 K, 423 K, and 473 K for 5 min, respectively. All spectra were recorded using FTIR spectrometer within the scan range of 500–1400 cm^{-1} with a resolution of 5 cm^{-1}.

Field Emission Scanning Electron Microscopy (FESEM) equipped with the elemental distribution mapping (JEOL JSM7800F Electron Microscope) was performed in order to identify the morphological structural of metal-based catalysts as well as its metal distribution. Transmission electron micrograph (TEM) observation was executed on TEM Philips CM12. Prior to the analysis, catalyst was dispersed in ethanol, dropped onto a porous, amorphous carbon grid, and dried.

For the evaluation of coke deposition on the spent Ni/F-SBA-15 catalysts, it was done by thermogravimetric analyzer (TGA, Q500, TA Instruments), operated under 20%O_2/80% N_2 at 1173 K with the heating rate of 5 K min^{-1}.

Catalytic testing

The CO_2 methanation over catalysts was performed in a stainless steel fixed-bed reactor at the temperature of 673 K, specific gas hourly space velocity (GHSV) of 24,900 mL g^{-1} h^{-1} and H_2/CO_2 ratio of 4/1. Prior to the reaction, 0.2 g of sample was mixed with the quartz wool, put in the middle of the reactor and degassed in a flow of H_2 stream ($F_{Hydrogen} = 20$ mL min^{-1}) for 1 h at 973 K, followed by cooling down to the desired temperature. Then, gaseous reactants of H_2 and CO_2 were fed into the reactor and the composition of gaseous effluent was analyzed with an Agilent gas chromatography equipped with a GS-Carbon PLOT column and a thermal conductivity detector (TCD). The calculation on CO_2 conversion, CH_4 selectivity, and CH_4 yield were done based on the following equations:

$$CO_2 \text{ conversion, } X_{CO_2}(\%) = \frac{F_{CO_2,in} - F_{CO_2,out}}{F_{CO_2,in}} \times 100\% \quad (3)$$

$$CH_4 \text{ selectivity, } S_{CH_4}(\%) = \frac{F_{CH_4,out}}{F_{CO_2,in} - F_{CO_2,out}} \times 100\% \quad (4)$$

$$CH_4 \text{ yield, } Y_{CH_4}(\%) = \frac{X_{CO_2} \times S_{CH_4}}{100\%} \quad (5)$$

where F is the molar flow rate for the particular compound in mol s^{-1}. The turnover number (TON) was calculated as number of moles of CH_4 produced/mole of catalyst. Meanwhile, the turnover frequency (TOF) was computed as the TON/time of reaction.

Results and discussion

Characterization of the synthesized catalysts

The characterization of synthesized F-SBA-15 and Ni/F-SBA-15 catalysts with the different amount of Ni loadings were carried out using XRD, BET, ICP-MS, FTIR, FESEM-EDX, TEM, and in-situ FTIR adsorbed pyrrole. Fig. 1 indicates the (A) low-angle and (B) wide-angle XRD patterns of F-SBA-15 and Ni-

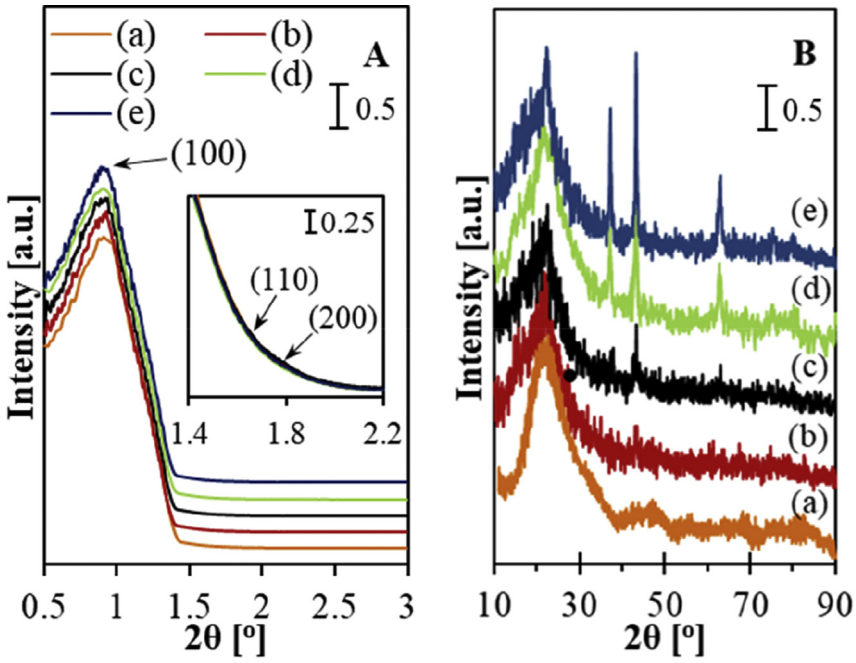

Fig. 1 – XRD patterns for (A) low-angle and (B) wide-angle of (a) F-SBA-15, (b) 1%Ni/F-SBA-15, (c) 3%Ni/F-SBA-15, (d) 5%Ni/F-SBA-15, and (e) 10%Ni/F-SBA-15.

based F-SBA-15 (1, 3, 5, and 10 wt%) catalysts. The low-angle XRD patterns of F-SBA-15 and all Ni-based F-SBA-15 catalysts (Fig. 1) displayed three main diffraction peaks indexed as (100), (110), and (200) reflections of typical two-dimensional, attributing to the presence of hexagonally ordered mesostructures (*p*6mm) with uniform and high quality of mesoporous packing [17]. The Ni inclusion did not markedly alter the ordered mesostructured of F-SBA-15 support structure due to no shift in the peaks and no decreasing intensities were observed with the inclusion of metal, even with the increasing of Ni loading. The results indicated no structural degradation of F-SBA-15 support due to a highly ordered structural arrangement of F-SBA-15 support. As displayed in Fig. 1(B), F-SBA-15 and all Ni-based F-SBA-15 catalysts exhibited the broad diffraction peak in the region of 10.0–30.0°, revealing the appearance of SiO_2 framework in the support. Besides, there are five main diffraction peaks at 37.3°, 43.2°, 62.9°, 75.4°, and 79.3° possessed by all Ni/F-SBA-15 catalysts, which are corresponding to face-centred cubic (FCC) crystalline NiO structure [18]. The intensity of the five main diffraction peaks increased upon the increasing of Ni loading from 1 to 10%, followed the order of 1%Ni/F-SBA-15 < 3%Ni/F-SBA-15 < 5%Ni/F-SBA-15 < 10%Ni/F-SBA-15, revealing the highest accessibility and incorporation of NiO crystallites onto F-SBA-15 support at 10 wt%, in agreement with Aziz et al. [14] for Ni/MSN catalysts.

The NiO crystallites size was determined based on the Scherrer equation (Eq. (2)) and their results are shown in Table 1. Despite the increasing Ni loading onto F-SBA-15 support from 1 to 5%, NiO crystallites size slightly increased ranging between 7.99 nm and 8.92 nm, representing to a higher quantity and homogenous dispersion of NiO crystallites onto the framework of F-SBA-15 support [14]. However, a further increment in the amount of Ni loading (10 wt%) onto the structure of F-SBA-15 support resulted to a drastically enlargement of NiO crystallites size (17.73 nm) in accordance to an aggregation of NiO crystallites located on the outer surface of F-SBA-15. This phenomenon might be due to the limited access of the NiO crystallites entering the framework of F-SBA-15 or partial interruption of F-SBA-15 structure resulted from the bulky Ni nanoparticles and thus exhibited towards a poorer metal deposition together with a weaker metal-support interaction.

By referring to the previous study by Setiabudi et al. [19], it was reported that a lower percentage crystallinity or partially collapse of Pt-HZSM5 structure at higher iridium loading might be related to a bulk iridium phase, corresponding to a limitation in available spaces for metal deposition, and thus resulted in a poorer metal dispersion and weaker metal-support interaction. Similar observation was also described by Stekrova et al. [20]. They claimed that the formation of metal crystallites with a bigger size might be due to the existence of a weaker interaction between the mixed oxide supports and metal, and thus decreased the homogeneity of metal deposition onto the surface of those supports.

The properties of F-SBA-15 and Ni-based F-SBA-15 are listed in Table 1. BET surface area of F-SBA-15 support was 284.0 $m^2\ g^{-1}$. With an increase of the Ni loading into F-SBA-15 (1–10 wt%), the BET surface area was found to decrease simultaneously from 126.0 to 62.3 $m^2\ g^{-1}$, respectively, attributing to F-SBA-15 support was incorporated by nickel oxides [21] which could enhance the metal-support interaction. Moreover, the readings of the pore volume of catalysts inconsistently decreased (0.34–0.19 $cm^3\ g^{-1}$) upon the incorporation of Ni loading from 1 to 5 wt%, indicating the pore blockage with Ni species. However, excess Ni loading onto F-SBA-15 support (10 wt%) significantly increased its pore volume (0.24 $cm^3\ g^{-1}$) as compared to 5%Ni/F-SBA-15,

Table 1 – Physical properties of F-SBA-15 and Ni/F-SBA-15 catalysts.

Catalysts	Surface area ($m^2\ g^{-1}$)	Pore volume ($cm^3\ g^{-1}$)[a]	Pore diameter (nm)	NiO crystallite size (nm)[b]		Intended Ni loadings (%)	Ni loadings (%)[c]
				Fresh	Spent		
F-SBA-15	284.0	0.34	5.3	–	–	–	–
1%Ni/F-SBA-15	126.0	0.20	6.1	7.99	8.44	1	1.03
3%Ni/F-SBA-15	122.1	0.22	6.8	8.86	9.51	3	2.99
5%Ni/F-SBA-15	120.3	0.19	7.0	8.92	9.02	5	5.01
10%Ni/F-SBA-15	62.3	0.24	8.7	17.73	18.39	10	10.07

[a] Obtained from Barret-Joyner-Halenda (BJH) desorption method.
[b] Calculated from XRD result using Scherrer equation.
[c] Determined from ICP-MS analysis.

representing the interruption of metal-support incorporation with a poorer metal dispersion and higher insertion of 10 wt% of Ni particles into the pore mouth of F-SBA-15 support which then caused the metal agglomeration, significant wall contraction and pores' expansion [15,21]. Meanwhile, the growth in pore size increased gradually from 6.1 nm (1%Ni/F-SBA-15) to 8.7 nm (10%Ni/F-SBA-15) upon the increasing of Ni loadings. This circumstance suggested the enlargement of the pores size resulted from the increased Ni atoms substitution and incorporation over the Si atoms within the F-SBA-15 framework [22].

The ICP-MS analysis has also been added and showed in Table 1 in order to quantify the actual Ni loadings onto the F-SBA-15 and also compared with the intended Ni loadings. As observed, the quantification of exact amount of Ni loadings (1, 3, 5, and 10%) onto F-SBA-15 support was nearly identical with the reading of intended Ni loadings (1.03, 2.99, 5.01, 10.07%). This phenomenon implied that Ni metals were probably successfully distributed and dispersed onto F-SBA-15 framework upon the inclusion of the different amount of Ni loadings occurred, in compliance with the previous study that reported by Mondal et al. [23] on $Ni/CeO_2–ZrO_2$ and $Rh–Ni/CeO_2–ZrO_2$ catalyst for H_2 production.

To investigate the functional groups and metal-support interaction of Ni/F-SBA-15 catalysts prepared at different amount of Ni loadings (1, 3, 5, and 10 wt%), FTIR spectra were collected in the wavelength ranging from 500 to 1400 cm^{-1}. As displayed in Fig. 2(A), the bands appeared at 3450, 1635, 1060, 961, and 801 cm^{-1}, indicated the presence of –OH stretching, adsorbed H_2O molecules retained by siliceous materials, Si–O–Si asymmetric stretching, external Si–OH groups, and Si–O–Si symmetric stretching bonds in the framework, respectively [15,24–26]. The inclusion of Ni from 1 to 10 wt% slightly altered the intensity of the band at 961 cm^{-1} and become enveloped in the band of 1060 cm^{-1}, revealing the isomorphous replacement of surface silanol groups (Si–OH) stretching with Ni species forming Si–O–Ni. Interestingly, it could be found that the highest quantity with the strongest metal-support interaction (Si–O–Ni) was exhibited by 5%Ni/F-SBA-15 as it possessed the less intense peak at 961 cm^{-1} and

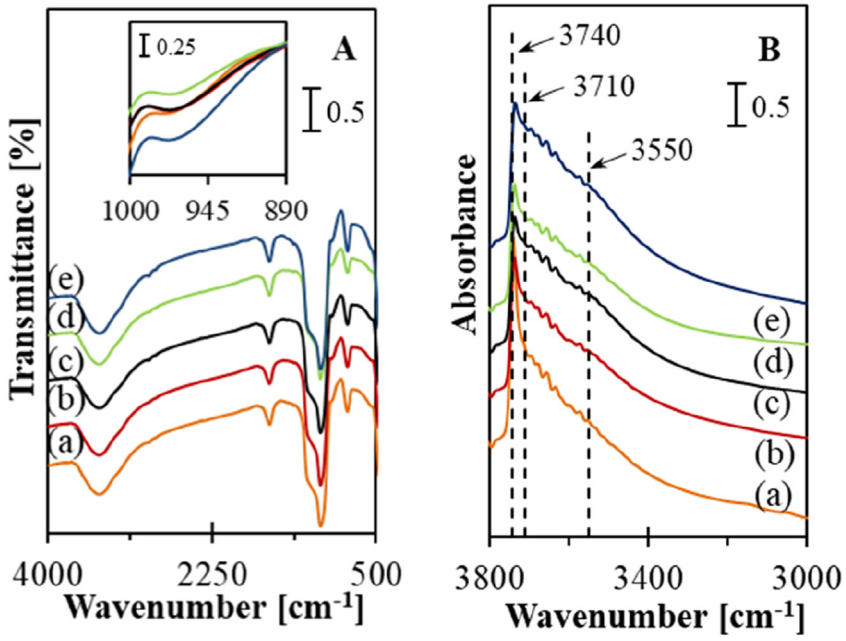

Fig. 2 – (A) FTIR spectra of KBr pellet method and (B) activated catalysts of (a) F-SBA-15, (b) 1%Ni/F-SBA-15, (c) 3%Ni/F-SBA-15, (d) 5%Ni/F-SBA-15, and (e) 10%Ni/F-SBA-15.

become enveloped in the band of 1060 cm^{-1} (inset Fig. 2(A)) compared with other catalysts. However, higher Ni loadings (more than 5 wt%) onto F-SBA-15 support lowered the metal-support interaction, resulting the agglomeration of abundance Ni phase. The evidence of the Si–O-Metal formation via the changes in the vibration of Si–OH groups at the band of 961 cm^{-1} was also reported by Jusoh et al. [27] for ZnO/MSN catalyst.

In addition, reduced F-SBA-15 and Ni/F-SBA-15 catalysts possessed a sharp peak at 3740 cm^{-1} with a shoulder at 3710 cm^{-1} (Fig. 2(B)), attributing to the appearance of terminal (isolated) and internal silanol group [28], respectively. The incorporation of Ni species from 1 to 10 wt% onto F-SBA-15 support significantly decreased the intensity of the band at 3740 cm^{-1}, which might be owing to the perturbation of silica framework with Ni species [29]. Meanwhile, the broad band at 3550 cm^{-1} was attributed to structural defect and/or vicinal hydroxyl groups [30]. It could be observed that increasing Ni loadings onto F-SBA-15 influenced the minor structural defect and/or vicinal hydroxyl groups, suggesting the promising properties of fibrous structure type with highly ordered mesoporous structured of F-SBA-15 support, allowed towards a higher incorporation and better dispersion of Ni particles into the silica framework and pore channels of support. However, upon the interaction with Ni at 10 wt%, the structural defect and/or vicinal hydroxyl groups were slightly reduced, assigning to the perturbation of F-SBA-15 framework due to a bulk interaction with Ni species.

The FESEM elemental mapping image of 5%Ni/F-SBA-15 is illustrated in the inset Fig. 3(A) as to determine its surface morphology and metal dispersion. It could be clearly proved that most of the Ni species were homogenous and well-dispersed onto the uniform rod-like shape of F-SBA-15 with highly aligned of the fibrous structure covering at the outer surface (Fig. 3(A)), resulting to a greater Si–O–Ni bond with a stronger metal-support interaction in 5%Ni/F-SBA-15. It was in accordance with the earlier postulation in FTIR results, whereby it could be noticed that 5%Ni/F-SBA-15 exhibited the less intense peak at band of 961 cm^{-1} and became enveloped in the band of 1060 cm^{-1} than other Ni-based F-SBA-15 catalysts (inset Fig. 2(A)) evidencing the highest quantity and strength between metal and support interaction (Si–O–Ni) in 5%Ni/F-SBA-15 framework. This phenomenon was most probably due to the promising effect of the fibrous support which allowed a better dispersion and higher crystallinity of Ni species at an optimum insertion of 5% Ni loading. A comparable observation was also found by Firmansyah et al. [13], who explored the incorporation and dispersion of platinum (Pt) onto the silica framework of fibrous ZSM-5 (F-ZSM-5). Fig. 3(B) indicates the TEM image of the closed up single particle of F-SBA-15. The lattice structure of SBA-15 was seen with the fibrous structure aligned on the external surface, proven that the SBA-15 had been modified into fibrous SBA-15 (F-SBA-15). It was in compliance with the previous assumption in FESEM-EDX (Fig. 3(A)) whereby the F-SBA-15 were covered with the fibrous structure on the external surface.

The basicity of all Ni/F-SBA-15 catalyst was investigated by in-situ FTIR adsorbed pyrrole and their spectra are shown in Fig. 4. The peak at 3530 cm^{-1} and 3410 cm^{-1} revealed N–H band from pyrrole molecules (C_4H_4NH) in the gas phase [31] and physisorbed pyrrole in the liquid-like state [32], respectively. In the spectral region of 3475–3200 cm^{-1}, the main broad band could be assigned to the formation of C_4H_4NH–O bridges with basic oxygen, indicating N–H stretching vibrations of chemisorbed pyrrole (C_4H_4NH) interacted with the basic sites of framework oxygen atoms. The interaction between perturbed N–H stretch of pyrrole and the basic sites of the catalysts could be investigated from the band of 3467 cm^{-1} [14]. It was recognized that the intensity at 3467 cm^{-1} was increased upon increasing Ni loadings from 1 to 5 wt%, attributing to an addition of Ni loadings up to 5 wt% provided more active basic sites on the framework of the catalyst that chemically interact with the pyrrole molecules. The high basic sites of catalyst resulted to a high adsorption of CO_2 gases, thus subsequently affected its reactivity with another gaseous reactant, H_2. A lower tendency of pyrrole to the blocking effect observed in 5%Ni/F-SBA-15 catalyst might also correspond to the higher quantity and better Ni dispersion [33]. Notably, the number of basic sites at higher Ni loadings (10 wt%) slightly reduced due to a poorer Ni dispersion upon bulk Ni phase. In addition, it was related to a limited availability and accessibility of the pyrrole adsorption sites to chemically react with the basic sites of 10%Ni/F-SBA-15, corresponding to the limited availability of basic oxygen in the framework of support. This phenomenon was in accordance with Kučera et al. [34], who previously described that the basicity of ZSM-5 was highly correlated with the presence of framework oxygen atoms, which are the key element for contributing good

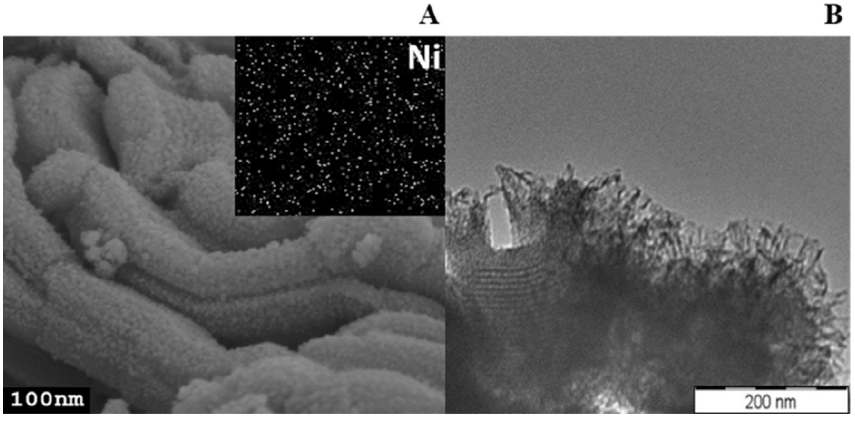

Fig. 3 – (A) FESEM-EDX image for 5%Ni/F-SBA-15. (B) TEM image of the closed up single particle of F-SBA-15.

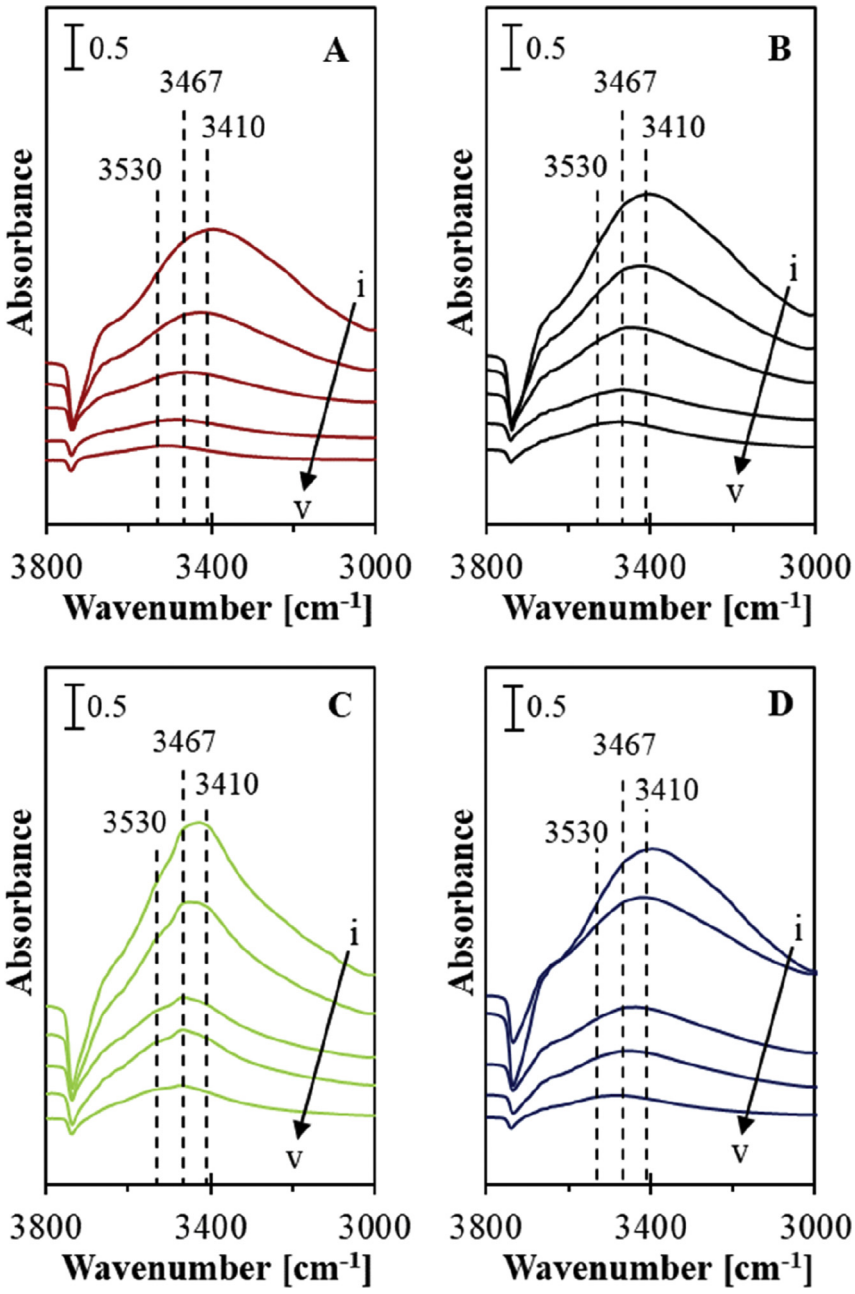

Fig. 4 – IR spectra of pyrrole adsorbed on the reduced Ni/F-SBA-15 catalysts, exposed to 2 Torr pyrrole at room temperature, followed by evacuated at (i) room temperature, (ii) 323, (iii) 373, (iv) 423, and (v) 473 K for (A) 1%Ni/F-SBA-15, (B) 3%Ni/F-SBA-15, (C) 5%Ni/F-SBA-15, and (D) 10%Ni/F-SBA-15 catalysts.

catalytic activity. However, the intensities of the bands of all supported metal catalysts with the different amount of metal loadings (1–10 wt%) slightly decreased upon the heating process from 323 K to 473 K, indicating the pyrrole was being removed from the basic sites of catalyst owing to weak pyrrole-SiO_2 interaction [32].

Catalytic behavior of synthesized catalysts

The CO_2 methanation activity over all Ni supported onto F-SBA-15 with the different amount of Ni loadings (1, 3, 5, and 10 wt%) are shown in Fig. 5(A–C). As presented in Fig. 5 (A-C), increment of Ni loadings (1–5 wt%) resulted in an increasing CO_2 conversion, CH_4 selectivity, and CH_4 yield. This phenomenon was due to the enhancement of CO_2 and H_2 dissociation upon the increasing metal sites contained in the metal-based catalyst which then impacted towards an ascending performance of the metal-based catalysts [33,35]. Without the metal sites, the performance of the catalyst becomes not too active as the supported metal catalyst. From this study, it represented that the most excellent behavior towards CO_2 methanation was possessed by 5%Ni/F-SBA-15, whereby it exhibited 98.9% CO_2 conversion, 99.6% CH_4 selectivity, and 98.5% CH_4 yield at 673 K for 6 h time-on-stream.

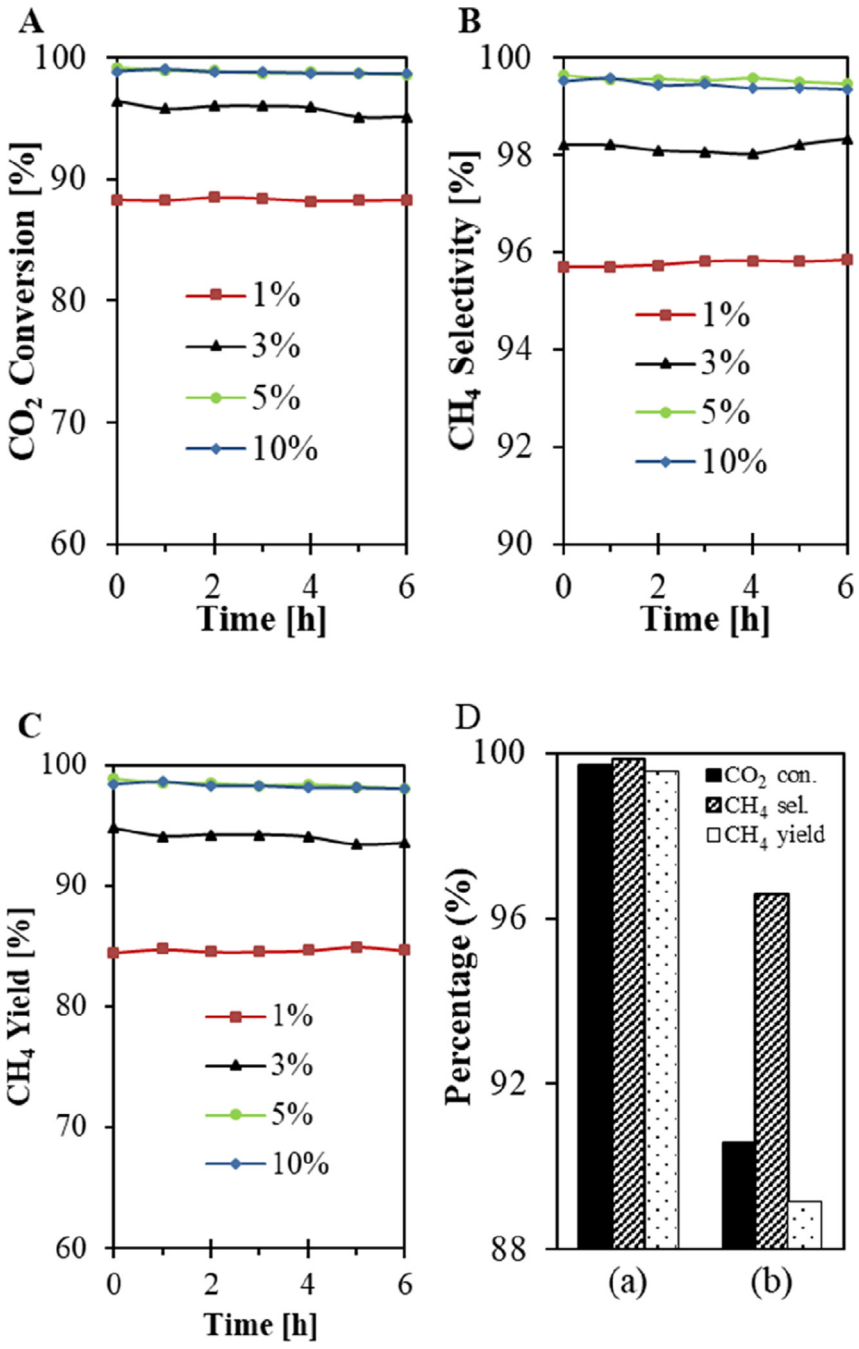

Fig. 5 – (A–C) Catalytic performances of all different Ni loadings onto F-SBA-15 support (1, 3, 5, and 10%) towards CO_2 methanation. Reaction conditions: T = 673 K, GHSV = 24,900 mL g^{-1} h^{-1}, stoichiometric H_2/CO_2 = 4/1, time-on-stream = 6 h. (D) Comparison performance of (a) 5%Ni/F-SBA-15 towards CO_2 methanation with (b) 5%Ni/SBA-15.

Table 2 summarizes the TON and TOF values for the CO_2 methanation on F-SBA-15 with different Ni loadings, in which the maximum TOF values increased with the order of 1% (0.93 s^{-1}) < 3% (1.20 s^{-1}) < 10% (1.61 s^{-1}) < 5% (1.63 s^{-1}). Additionally, the TOF value for 5%Ni/F-SBA-15 was compared with the previous reported catalysts [21,36–38] over CO_2 methanation (as shown in Table 3), and was found to be the highest TOF value obtained than the previous reported data. It might be due to a favorable structure of 5%Ni/F-SBA-15 whereby numerous substitution of silanol groups with larger quantity and better Ni dispersion and thus, resulted to a stronger metal-support interaction. However, the activity of catalyst started to decline upon the excess Ni loadings at 10 wt% in which a slightly declined in the CH_4 selectivity was observed, representing the occurrence of Ni agglomeration began to start. This phenomenon might not be due to the smaller specific surface area of F-SBA-15 support, but it was relatively related with the limitation substitution of Ni species with the silanol groups of F-SBA-15 support upon the bulk Ni phase, attributing to a poorer Ni distribution and weaker metal-

Table 2 – Summary of the maximum TON and TOF values for the CO_2 methanation on F-SBA-15 with different Ni loadings (1%, 3%, 5%, 10%). Operating conditions: temperature = 673 K, GHSV = 24,900 mL g^{-1} h^{-1} and H_2/CO_2 ratio = 4/1.

Catalysts	TON	TOF (max) (s^{-1})
1%Ni/F-SBA-15	20,088	0.93
3%Ni/F-SBA-15	25,920	1.20
5%Ni/F-SBA-15	35,208	1.63
10%Ni/F-SBA-15	24,774	1.61

Table 3 – Summary of the maximum TOF values for the CO_2 methanation on different catalysts.

Catalysts	Reaction temperature (K)	TOF (max) (s^{-1})	Reference
5%Ni/MSN	573	1.61	[21]
5%Ni/MCM-41		1.41	
5%Ni/HY		1.21	
5%Ni/SiO_2		1.06	
5%Ni/α-Al_2O_3		0.69	
5%Ru/Al_2O_3	573	0.34	
2%Ru/Al_2O_3		0.28	[36]
1%Ru/Al_2O_3		0.23	
75%Ni/Al_2O_3		0.013	[37]
75%Ni25Fe%/Al_2O_3	523	0.033	
75%Ni25Co%/Al_2O_3		0.017	
75%Ni25Cu%/Al_2O_3		0.004	
Rh/Al_2O_3	534	0.016	[38]
Rh–STF	665	0.0102	
Rh–LSF	712	0.0109	
1%Ni/F-SBA-15	673	0.93	This study
3%Ni/F-SBA-15		1.20	
5%Ni/F-SBA-15		1.63	
10%Ni/F-SBA-15		1.61	

support interaction. It could be summarized that an optimum amount of Ni loadings onto the support with better deposition and stronger metal-support interaction was considered as an crucial factor in enhancing towards an excellent activity of CO_2 methanation, in agreement with Gouveia et al. [39], who discovered about the influence of Ni loadings (5–25 wt%) incorporated onto SBA-15 support for the combined steam methane reforming (SMR) and water gas shift (WGS) reaction.

The catalytic performance of 5%Ni/F-SBA-15 was compared with the Ni supported onto the conventional SBA-15 support (5%Ni/SBA-15) and their comparisons were illustrated in Fig. 5(D). As observed, it was significantly evidenced that the 5%Ni/F-SBA-15 possessed a higher and efficient catalytic behavior towards CO_2 methanation (T = 673 K, CO_2 conversion = 99.7% and CH_4 yield = 98.2%) as compared with 5%Ni/SBA-15 (T = 673 K, CO_2 conversion = 91.1% and CH_4 yield = 87.5%). This observation demonstrated that the 5%Ni/F-SBA-15 was superior to 5%Ni/SBA-15 owing to its high potentiality of favorable properties of F-SBA-15 towards a better and homogenous metal dispersion with a stronger metal-support interface which then resulted to an excellent catalytic activity as well as might hinder the occurrence of catalyst deactivation. It was in consistence with Firmansyah et al. [13] who investigated about Pt/FZSM-5 for cumene hydrocracking.

Catalytic stability of catalysts

Fig. 6(A) shows the long-term stability test of the different amount of Ni loadings onto F-SBA-15 catalysts at 673 K. It was observed that the most optimum and better stability of catalyst was exhibited by 5%Ni/F-SBA-15, whereby it remained active in CO_2 conversion during 120 h time-on-stream. This phenomenon might be due to the numerous substitution of silanol groups with a larger quantity of Ni species, thus resulted in a better and homogenous Ni deposition together with a higher strength of metal-support interaction among Ni/F-SBA-15 for CO_2 methanation. Apart from that, it might inhibit metal sintering during the reaction as well as promoted towards an excellent catalytic performance and stability of CO_2 methanation over 5%Ni/F-SBA-15. Razzaq et al. [40] had also investigated that the superior catalytic performances and stabilities towards CO and CO_2 methanation over Co_4N/γ-Al_2O_3 catalyst were highly related with the resistance of metal sintering and carbon deposition.

For 10%Ni/F-SBA-15, a slight reduction of catalytic stability of catalyst was observed, which closely related with the limitation substitution of silanol groups at a higher amount of Ni loading, thus reduced Ni dispersion as well as weakened the metal-support interaction. This observation was also discovered by Junke et al. [41] and they reported that the factors which highly influenced towards the favorable catalytic performance of catalysts were due to a better and homogenous metal dispersion as well as stronger metal-support interaction. In contrast, the occurrence of poorer catalytic stability of catalyst might be due to the poorer metal deposition and weaker metal-support interaction which triggered towards Ni agglomeration on the surface of support when reacted at the elevated reaction temperature. The Ni particles might be lifted easily from the support resulting the negative effects of coke formation and catalyst deactivation [41]. On the other hand, with regards to Aziz et al. [14], decreasing in catalytic behavior and stability of CO_2 methanation over Ni-promoted MSN might also be due to the formation of coke which originated from CO disproportionation as well as from CH_4 decomposition on the surface of catalyst during the activity.

After 120 h catalytic stability testing, the spent catalysts were then characterized using XRD analysis as to further study the reduction of NiO into Ni^0 crystallites deposited onto the surface of the spent catalysts. As displayed in Fig. 6(B), all spent Ni/F-SBA-15 catalysts possessed main broad diffraction peak in the region of 10.0–30.0° and the three diffraction peak positions approximately at 44.3°, 52.5°, and 76.8° which were assigned to the presence of SiO_2 in the framework of support and the appearance of Ni^0 crystallite on the surface of Ni-based catalysts [28,42], respectively. Those peaks became more intense upon the increment of Ni loadings (1–10 wt%) after the 120 h of reaction towards CO_2 methanation. Their intensities increased in a sequence of 1%Ni/F-SBA-15 < 3%Ni/F-SBA-15 < 5%Ni/F-SBA-15 < 10%Ni/F-SBA-15, revealing that the most intense peak of Ni^0 crystallite was possessed by 10%Ni/F-SBA-15. This phenomenon could be described by the formation of Ni^0 crystallites species deposited on the outer surface of the spent catalyst, indicating the poorer metal distribution and weaker metal-support interaction upon the abundance of Ni phase. No

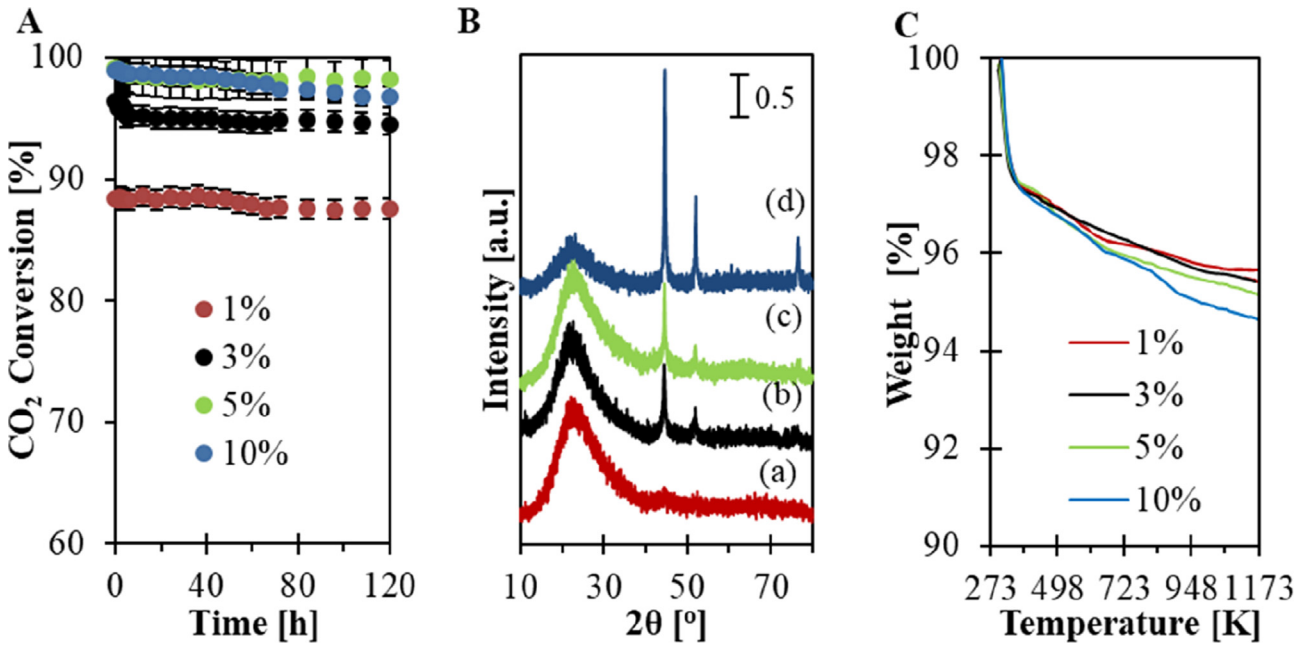

Fig. 6 – (A) Long-term stability test of fresh (a) 1%Ni/F-SBA-15, (b) 3%Ni/F-SBA-15, (c) 5%Ni/F-SBA-15, and (d) 10%Ni/F-SBA-15 catalysts. (B) XRD and (C) TGA analysis of all spent catalysts. Reaction conditions: T = 673 K, GHSV = 24,900 mL g^{-1} h^{-1}, stoichiometric H_2/CO_2 = 4/1, time-on-stream = 120 h. Error bars reveal the standard error by mean of three replicates of the experiment taking over in this study.

diffraction peaks of NiO crystallite were detected among all spent Ni/F-SBA-15 catalyst, attributing to the occurrence of completely NiO reduction into Ni⁰ crystallite after the reduction at a higher reaction temperature.

The Ni⁰ crystallite size of each spent supported Ni catalysts were determined by the Scherrer equation (Eq. (2)) and the readings are summarized in Table 1. The obtained results showed the readings of 8.44 nm, 9.51 nm, 9.02 nm, and 18.39 nm for the spent 1%Ni/F-SBA-15, 3%Ni/F-SBA-15, 5%Ni/F-SBA-15, and 10%Ni/F-SBA-15, respectively. It showed that spent 10%Ni/F-SBA-15 was more prone towards Ni sintering, indicating the poorest Ni distribution and weaker metal-support interaction which allowed the nucleation and growth of metallic Ni crystallites, in parallel with the previous assumptions reported by Junke et al. [41]. In addition, a generation of carbon deposition was expected to occur in 10%Ni/F-SBA-15 upon the formation of largest Ni⁰ crystallite size. According to Taherian et al. [43], they suggested that an assembly of Co species with large crystallite size on the support might cause an occurrence of metal agglomeration during the dry reforming of CH_4 attributable to relatively weak metal-support interaction, and thus triggered towards sintering activity along with more carbon deposition onto the support surface. Therefore, it was reasonable to conclude that higher Ni loading (10 wt%) for Ni–F-SBA-15 generated the instability of metal crystallite with larger size whereby the Ni⁰ crystallites were being lifted easily from the F-SBA-15 due to weak metal-support interaction, and thus expected to stimulate the carbon species deposition. Apart from that, the carbon species might block the active sites of Ni which then could decline its catalytic activity and stability towards CO_2 methanation (Fig. 6).

Fig. 6(C) indicates the TGA profiles of all spent Ni/F-SBA-15 catalysts for 120 h time-on-stream. The initial weight loss appeared at a temperature below than 473 K attributing the dehydration of adsorbed H_2O [15], meanwhile, the gradual weight loss appeared at a temperature above than 673 K indicating the removal (oxidation) of carbon species [11,40]. There are two oxidation types of carbon species which known as amorphous carbon (673–773 K) and graphite carbon (>773 K) [28]. As shown in Fig. 6(C), an increase in Ni loadings (1–5 wt%) onto the framework of F-SBA-15 support slightly reduced the weight loss percentage, indicating the less significant formation of carbon species. However, no further decrement of weight loss percentage was noticed upon the introduction of higher metal loading (10 wt%), but it began to slightly increase the weight loss percentage of carbon species as compared with 5%Ni/F-SBA-15, implying the growth of carbon deposition. It might be due to a poorer metal distribution and dispersion, lower metal-support interaction, and lower amount of active basic sites of the catalyst upon the presence of bulk Ni species (10 wt%) onto the framework of F-SBA-15.

According to the analysis of spent catalyst, the highest resistance towards Ni sintering and the growth of coke formation were achieved at an optimum insertion of 5 wt% Ni loading due to a homogenous and well-dispersed of Ni particles, stronger metal-support interaction, higher surface basicity of catalyst, and thus might be affected towards a superior catalytic stability and minimized the growth of coke formation on the catalyst surface. It can be noticed that the better metal deposition, higher strength of metal-support interaction, together with a higher amount of active basic sites were considered as the important factors for possessing

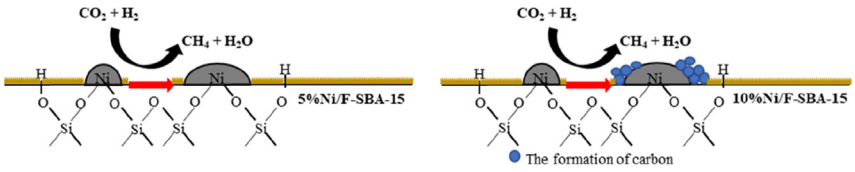

Fig. 7 – Plausible mechanism of Ni/F-SBA-15 towards CO_2 methanation.

an excellent long-term catalytic activity and stability as well as minimizing the growth of coke deposition, in compliance with the previous studies [15,28,44].

By referring to the obtained characterization results and reported assumptions in the above, the proposed reaction pathway of Ni/F-SBA-15 incorporated with the different Ni loadings (1–10 wt%) for CO_2 methanation was presented in Fig. 7. Even though the possible intermediate products of CO_2 methanation over metal-based catalyst was still under debatable by several researchers [21,45], it was proposed that the better and homogenous metal dispersion, stronger interaction between support with bulk metal species, and higher amount of active basic sites on the supported metal catalyst were vital for an efficient CO_2 methanation activity. In the present study, the increasing Ni loading onto the channels of fibrous support from 1 wt% to 5 wt% enhanced the catalytic performances towards CH_4 production over the Ni/F-SBA-15, indicating the most promising characteristics and superior performance of 5%Ni/F-SBA-15. It was proven that the fibrous morphology of mesoporous silica support (Fig. 3) provides more spaces for Ni incorporation (Si–O–Ni) with a better and homogenous metal dispersion (inset Fig. 3), higher formation of active basic sites upon the addition of Ni loadings onto the support, and strengthen the metal-support interaction (Fig. 2). Apart from that, it might allow towards an efficient dissociation of H_2 and CO_2 into the CH_4 production, in compliance with the study explored by Aziz et al. [21]. While for an excess amount of Ni loading (10 wt%), it resulted to the formation of carbon due to bulk coverage of Ni species onto F-SBA-15 framework which lowered the metal-support interaction. It could be summarized that the most important and attractive key factors for achieving excellent catalytic performance and stability of CO_2 methanation over metal-based catalyst are synergistic effects of Ni loadings onto the support with a higher quantity of Si–O–Ni bond, better and homogenous Ni dispersion, stronger metal-support interaction, and higher amount of active basic sites provided.

Conclusion

In conclusion, developing the new promising characteristics of Ni/F-SBA-15 with the varied amount of Ni loadings were discovered and synthesized. Their textural properties were investigated by XRD, BET, ICP-MS, FTIR, FESEM-EDX, TEM, and in-situ FTIR adsorbed pyrrole. It was found that the most promising and optimum amount of Ni loadings to be incorporated and dispersed onto F-SBA-15 support for CH_4 production was at 5 wt%. 5%Ni/F-SBA-15 possessed an excellent catalytic performance and stability with no deactivation up to 120 h time-on-stream. Only small amount of Ni sintering was observed whereby a smaller nucleation and growth of metallic Ni^0 crystallites occurred due to a better and homogenous NiO dispersion accompanied by stronger the metal-support interaction, in compliance with the XRD result over the spent catalyst. Addition of 5 wt% Ni loading onto the F-SBA-15 support provided the higher presence of active basic sites on the catalyst surface which then might possess better stability even after 120 h time-on-stream. However, a trivial reduction in the catalytic performance and stability of CO_2 methanation was achieved by 10%Ni/F-SBA-15 due to its limitation spaces and substitution of Ni species with the silanol groups of F-SBA-15 support upon the bulk Ni phase, attributing to a poorer Ni distribution and weaker metal-support interaction. The agglomeration of NiO crystallites might cover the active basic sites of the surface of the catalyst which then continuously declined the stability of the catalyst towards CO_2 methanation after 120 h time-on-stream. The coke deposition might also occur onto the surface of 10%Ni/F-SBA-15, as proven by the TGA analysis.

Acknowledgement

This work was financially supported by the Ministry of Education Malaysia via Fundamental Research Grant Scheme (RDU150126) and Research Acculturation Grant Scheme (RDU151414). In addition, the authors would like to acknowledge the Universiti Malaysia Pahang (UMP) for Postgraduate Research Grants Scheme (PGRS180303).

REFERENCES

[1] Levin DB, Chahine R. Challenges for renewable hydrogen production from biomass. Int J Hydrog Energy 2010;35:4962–9.
[2] Wang M, Ouyang L, Peng C, Zhu X. Synthesis and hydrolysis of $NaZn(BH_4)_3$ and its ammoniates. J Mater Chem A Mater Energy Sustain 2017;00:1–9.
[3] Mulewa W, Tahir M, Amin NAS. MMT-supported Ni/TiO_2 nanocomposite for low temperature ethanol steam reforming toward hydrogen production. Chem Eng J 2017;326:956–69.
[4] Stangeland K, Kalai D, Li H, Yu Z. The effect of temperature and initial methane concentration on carbon dioxide methanation on Ni based catalysts. Energy Procedia 2017;105:2016–21.
[5] Bacariza MC, Graça I, Bebiano SS, Lopes JM, Henriques C. Micro- and mesoporous supports for CO_2 methanation catalysts: a comparison between SBA-15, MCM-41 and USY zeolite. Chem Eng Sci 2018;175:72–83.
[6] Takahashi R, Sato S, Tomiyama S, Ohashi T, Nakamura N. Pore structure control in Ni/SiO_2 catalysts with both

macropores and mesopores. Microporous Mesoporous Mater 2007;98:107–14.
[7] Taguchi A, Schüth F. Ordered mesoporous materials in catalysis. Microporous Mesoporous Mater 2005;77:1–45.
[8] Zhao D, Feng J, Huo Q, Melosh N, Fredrickson GH, Chmelka BF, Stucky GD. Triblock copolymer syntheses of mesoporous silica with periodic 50 to 300 angstrom pores. Science 1998;279:548–52.
[9] Pan Q, Peng J, Wang S, Wang S. In situ FTIR spectroscopic study of the CO_2 methanation mechanism on $Ni/Ce_{0.5}Zr_{0.5}O_2$. Catal Sci Technol 2014;4:502–9.
[10] Kathiraser Y, Oemar U, Saw ET, Li Z, Kawi S. Kinetic and mechanistic aspects for CO_2 reforming of methane over Ni based catalysts. Chem Eng J 2015;278:62–78.
[11] Bukhari SN, Chin CY, Setiabudi HD, Vo DN. Tailoring the properties and catalytic activities of Ni/SBA-15 via different TEOS/P123 mass ratios for CO_2 reforming of CH_4. J Environ Chem Eng 2017;5:3122–8.
[12] Fihri A, Bouhrara M, Patil U, Cha D, Saih Y, Polshettiwar V. Fibrous nano-silica supported ruthenium (KCC-1/Ru): a sustainable catalyst for the hydrogenolysis of alkanes with good catalytic activity and lifetime. ACS Catal 2012;2:1425–31.
[13] Firmansyah ML, Jalil AA, Triwahyono S, Hamdan H, Salleh MM, Ahmad WFW, Kadja GTM. Synthesis and characterization of fibrous silica ZSM-5 for cumene hydrocracking. Catal Sci Technol 2016;6:5178–82.
[14] Aziz MAA, Jalil AA, Triwahyono S, Saad MWA. CO_2 methanation over Ni-promoted mesostructured silica nanoparticles: influence of Ni loading and water vapor on activity and response surface methodology studies. Chem Eng J 2014;260:757–64.
[15] Setiabudi HD, Lim KH, Ainirazali N, Chin SY. CO_2 reforming of CH_4 over Ni/SBA-15: influence of Ni loading on the metal-support interaction and catalytic activity. J Mater Environ Sci 2017;8:573–81.
[16] Cullity BD. Elements of X-Ray diffraction. 2nd ed. Read- Ing, MA: Addison-Wesley; 1978.
[17] Patil U, Fihri A, Emwas A-H, Polshettiwar V. Ilicon oxynitrides of KCC-1, SBA-15 and MCM-41 for CO_2 capture with excellent stability and regenerability. Chem Sci 2012;3:2224.
[18] Pudukudy M, Yaakob Z, Akmal ZS. Direct decomposition of methane over SBA-15 supported Ni, Co and Fe based bimetallic catalysts. Appl Surf Sci 2015;330:418–30.
[19] Setiabudi HD, Jalil AA, Triwahyono S. Ir/Pt-HZSM5 for n-pentane isomerization: effect of iridium loading on the properties and catalytic activity. J Catal 2012;294:128–35.
[20] Stekrova M, Rinta-Paavola A, Karinen R. Hydrogen production via aqueous-phase reforming of methanol over nickel modified Ce, Zr and La oxide supports. Catal Today 2017;304:143–52.
[21] Aziz MAA, Jalil AA, Triwahyono S, Mukti RR, Taufiq-Yap YH, Sazegar MR. Highly active Ni-promoted mesostructured silica nanoparticles for CO_2 methanation. Appl Catal B Environ 2014;147:359–68.
[22] Khajenoori M, Rezaei M, Meshkani F. Dry reforming over CeO_2-promoted Ni/MgO nano-catalyst: effect of Ni loading and CH_4/CO_2 molar ratio. J Ind Eng Chem 2015;21:717–22.
[23] Mondal T, Pant KK, Dalai AK. Catalytic oxidative steam reforming of bio-ethanol for hydrogen production over Rh promoted Ni/CeO_2-ZrO_2 catalyst. Int J Hydrog Energy 2015;40:2529–44.
[24] Karim AH, Jalil AA, Triwahyono S, Sidik SM, Kamarudin NHN, Jusoh R, Jusoh NWC, Hameed BH. Amino modified mesostructured silica nanoparticles for efficient adsorption of methylene blue. J Colloid Interface Sci 2012;386:307–14.
[25] Tomer VK, Devi S, Malik R, Nehra SP, Duhan S. Fast response with high performance humidity sensing of Ag-SnO_2/SBA-15 nanohybrid sensors. Microporous Mesoporous Mater 2016;219:240–8.
[26] Li S, Li K, Hao J, Ning P, Tang L, Sun X. Acid modified mesoporous Cu/SBA-15 for simultaneous adsorption/oxidation of hydrogen sulfide and phosphine. Chem Eng J 2016;302:69–76.
[27] Jusoh NWC, Jalil AA, Triwahyono S, Setiabudi HD, Sapawe N, Satar MAH, Karim AH, Kamarudin NHN, Jusoh R, Jaafar NF, Salamun N, Efendi J. Sequential desilication-isomorphous substitution route to prepare mesostructured silica nanoparticles loaded with ZnO and their photocatalytic activity. Appl Catal A Gen 2013;468:276–87.
[28] Sidik SM, Triwahyono S, Jalil AA, Aziz MAA, Fatah NAA, Teh LP. Tailoring the properties of electrolyzed Ni/mesostructured silica nanoparticles (MSN) via different Ni-loading methods for CO_2 reforming of CH_4. J CO_2 Util 2016;13:71–80.
[29] Gallo JMR, Bisio C, Gatti G, Marchese L, Pastore HO. Physicochemical characterization and surface acid properties of mesoporous [Al]-SBA-15 obtained by direct synthesis. Langmuir 2010;26:5791–800.
[30] Lercher JA, Jentys A, Cejka I, van Bekkum H, Corma A, Schuth F, editors. Introduction to zeolite science and practice. 3rd ed. Amsterdam: Elsevier; 2007. p. 452.
[31] Camarota B, Goto Y, Inagaki S, Onida B. Basic sites on periodic mesoporous organosilicas investigated by XPS and in situ FTIR of adsorbed pyrrole. Langmuir 2011;27:1181–5.
[32] Scokart PO, Rouxhet PG. Characterization of the basicity of oxides through the infrared study of pyrrole adsorption. J Chem Soc Faraday Trans 1 Phys Chem Condens Phases 1980;76:1476.
[33] Aziz MAA, Jalil AA, Triwahyono S, Sidik SM. Methanation of carbon dioxide on metal-promoted mesostructured silica nanoparticles. Appl Catal A Gen 2014;486:115–22.
[34] Kučera J, Nachtigall P, Kotrla J, Košová G, Čejka J. Pyrrole as a probe molecule for characterization of basic sites in ZSM-5: a combined FTIR spectroscopy and computational study. J Phys Chem B 2004;108:16012–22.
[35] Aldana PAU, Ocampo F, Kobl K, Louis B, Thibault-Starzyk F, Daturi M, Bazin P, Thomas S, Roger AC. Catalytic CO_2 valorization into CH_4 on Ni-based ceria-zirconia. Reaction mechanism by operando IR spectroscopy. Catal Today 2013;215:201–7.
[36] Li W, Wang H, Jiang X, Zhu J, Liu Z, Guo X, Song C. A short review of recent advances in CO_2 hydrogenation to hydrocarbons over heterogenous catalysts. RSC Adv 2018;8:7651–69.
[37] Ray K, Deo G. A potential descriptor for the CO_2 hydrogenation to CH_4 over Al_2O_3 supported Ni and Ni-based alloy catalysts. Appl Catal B Environ 2017;218:525–37.
[38] Thalinger R, Gotsch T, Zhuo C, Hetaba W, Wallisch W, Stoger-pollach M, Schmidmair D, Klotzer B, Penner S. Rhodium-catalyzed methanation and methane steam reforming reactions on rhodium-perovskite systems: metal-support interaction. ChemCatChem 2016;8:2057–67.
[39] Gouveia Gil A, Wu Z, Chadwick D, Li K. Ni/SBA-15 catalysts for combined steam methane reforming and water gas shift - prepared for use in catalytic membrane reactors. Appl Catal A Gen 2015;506:188–96.
[40] Razzaq R, Li C, Usman M, Suzuki K, Zhang S. A highly active and stable Co_4N/γ-Al_2O_3 catalyst for CO and CO_2 methanation to produce synthetic natural gas (SNG). Chem Eng J 2015;262:1090–8.
[41] Junke X, Wei Z, Jihui W, Zhaojing L, Jianxin M. Characterization and analysis of carbon deposited during the dry reforming of methane over $Ni/La_2O_3/Al_2O_3$ catalysts. Chin J Catal 2009;30:1076–84.

[42] Zhang J, Xin Z, Meng X, Tao M. Synthesis, characterization and properties of anti-sintering nickel incorporated MCM-41 methanation catalysts. Fuel 2013;109:693–701.
[43] Taherian Z, Yousefpour M, Tajally M. Catalytic performance of samaria-promoted Ni and Co/SBA-15 catalysts for dry reforming of methane. Int J Hydrog Energy 2017;42:24811–22.
[44] Zhao B, Chen Z, Chen Y, Ma X. Syngas methanation over Ni/SiO_2 catalyst prepared by ammonia-assisted impregnation. Int J Hydrog Energy 2017;42:27073–83.
[45] Wang X, Zhu L, Liu Y, Wang S. CO_2 methanation on the catalyst of Ni/MCM-41 promoted with CeO_2. Sci Total Environ 2018;625:686–95.